Proceedings of the 24th Conference on Mechanical Vibration and Noise
VIB2012
August 12-15, 2012, Chicago, Illinois, USA

DETC2012-71234

Dynamics Enhancements of Advanced LIGO Multi-Stage Active Vibration Isolators and Related Control Performance Improvement

[1,2] Fabrice Matichard* **[2] Ken Mason** **[2] Richard Mittleman** **[3] Brian Lantz**

[1] Ben Abbott **[2] Myron McInnis** **[4] Adrien LeRoux** **[2] Michael Hillard**

[4] Celine Ramet **[2] Sam Barnum** **[2] Andy Stein** **[2] Stephany Foley**

[5] Hugh Radkins **[2] Jeff Kissel** **[1,2] Sebastien Biscans** **[5] Vincent Lhuillier**

[1] Caltech
Pasadena, CA, USA

[2] MIT
Cambridge, MA, USA

[3] Stanford
Palo Alto, CA, USA

[4] LIGO Livingston Observatory
Livingston, LA, USA

[5] LIGO Hanford Observatory
Hanford, WA, USA

ABSTRACT

The control bandwidth and performance of active vibration isolation systems are usually directly related to the system dynamic characteristics. In this paper, we present results from a 4 years study carried out to improve the dynamical response and control performance on the two-stage isolator designed for Advanced LIGO detectors. The paper will focus on the platform's first stage to illustrate prototyping, optimization, final design and the experimental results obtained during this program. The system concept, architecture and prototype will be presented. The factors initially limiting the prototype's performance will be analyzed. Solutions based on sensors relocation, payload reduction, structural stiffening and passive techniques to damp the residual high frequency flexible modes will be presented. Experimental results obtained with the prototype will be compared with the system's final version. The series of improvement obtained help not only to increase the system's bandwidth, robustness and performance but also to simplify and speed up the control commissioning, which is very important for the Advanced LIGO project that will be using 5 of these platforms in each of its 3 detectors.

* Address correspondence to fabrice@ligo.mit.edu

1. INTRODUCTION

The new generation and upgrades of gravity wave detectors currently underway require unprecedented levels of isolation [1-4]. This paper focuses on the multi-stage platform that will provide the low frequency vibration and seismic isolation in the Advanced LIGO observatories [5-6]. The platform is made of two stages in series, each providing both passive and active isolation in all the directions of translation and rotation. This twelve-degree of freedom system carries as much as 800 kg of very sensitive payload, including the detector's test masses [7]. The active control scheme is made of a combination of 33 relative position sensors and seismometer signals to drive 12 electromagnetic actuators. It provides nanometer positioning resolution for optical alignment. The goal is to reach a seismic isolation factor of 15 at 0.1 Hz and a factor of 1000 at 10 Hz [8].

A 4-year study has been carried out to analyze the system prototype and to develop an optimal final version for the Advanced LIGO detectors. This study included both low and high frequency analysis. This paper presents the portion of the study dedicated to improving the high frequency performance. It will focus on the first stage to illustrate the process and the results obtained.

In the next section, the two-stage vibration isolator's concept, architecture and characteristics will be presented. The third section will present Initial Prototype (IP) results, and analyze the factors limiting the controls performance. It will describe improvements made on the platform, and the corresponding results of the Re-Engineered Prototype (RP).

The fourth section will present all the design solutions implemented in the Final Design (FD) to improve the systems dynamics. Experimental transfer functions and control loops showing the evolution and improvement of the system after each major phase of this program will be compared.

2. SYSTEM PRESENTATION

2.1. Two Stage Isolator Concept

The picture below illustrates the two-stage isolator concept. The base called Stage 0 supports Stage 1 with sets of horizontal and vertical springs. Stage 1 supports Stage 2 similarly. There are 3 sets of springs in between each stage, though only two sets are represented on this symbolic cross section drawing.

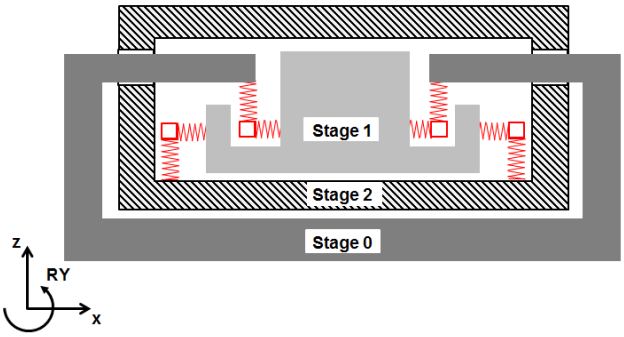

Figure 1. TWO-STAGE ISOLATOR CONCEPT.

The system has been designed to minimize the cross couplings between all directions of motion so that the system behaves as a two mass-spring system in each direction of translation and rotation, as illustrated in Figure 2 for a direction of translation. x_i, m_i, c_i and k_i are the motion, the mass, the natural damping (small) and the stiffness of the i^{th} stage; f_{xij} is the actuation force between the i^{th} and the j^{th} stage.

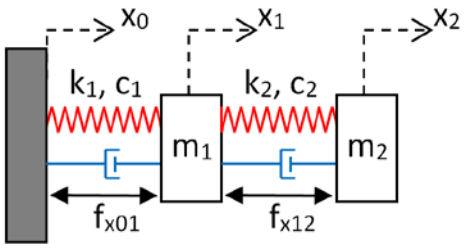

Figure 2. TWO MASS-SPRING-DAMPER MODEL.

Equation 1 gives the corresponding equations of motion. The base motion x_0 is the disturbance attenuated passively by the mass-spring system, and rejected actively by the control forces f_{x01} and f_{x12}.

$$M\begin{Bmatrix}\ddot{x}_1\\ \ddot{x}_2\end{Bmatrix} + C\begin{Bmatrix}\dot{x}_1\\ \dot{x}_2\end{Bmatrix} + K\begin{Bmatrix}x_1\\ x_2\end{Bmatrix} = A\begin{Bmatrix}x_0\\ \dot{x}_0\end{Bmatrix} - B\begin{Bmatrix}f_{x01}\\ f_{x12}\end{Bmatrix} \quad (1)$$

where:

$$M = \begin{bmatrix}m_1 & 0\\ 0 & m_2\end{bmatrix}, C = \begin{bmatrix}c_1 + c_2 & -c_2\\ -c_2 & c_2\end{bmatrix}, K = \begin{bmatrix}k_1 + k_2 & -k_2\\ -k_2 & k_2\end{bmatrix}$$

$$A = \begin{bmatrix}k_1 & c_1\\ 0 & 0\end{bmatrix}, \; B = \begin{bmatrix}1 & -1\\ 0 & 1\end{bmatrix}$$

Equation 2 describes the feedback control based on independent SISO control filters H_1 and H2.

$$F_{X01} = H_1(s)\, X_1 \; ; \quad F_{X12} = H_2(s)\; X_2 \quad (2)$$

where F_{X01}, F_{X12}, X_1 and X_2 are the Laplace transforms of f_{x01}, f_{x12}, x_1 and x_2 respectively.

In the next sections, analysis and results will be shown not only in the X directions but also in the others (Z, RY…), for which the theoretical behavior is similar.

2.2. System Architecture

Figure 3 shows a CAD picture of the actual system. The system's base (Stage 0) is shown in purple (0), the first active stage (Stage 1) is shown in cyan (1), and the second active stage (Stage 2) is shown in grey (2). Each stage is suspended with three triangular blades providing the vertical flexibility, and three vertical flexure rods providing the horizontal flexibility. (3) shows one of the three sets of blades between Stage 0 and Stage 1. (4) shows one of the three sets of blades between Stage 1 and Stage 2. The bottom plate of Stage 2 is an upside-down optical table designed to carry the Advanced LIGO optics.

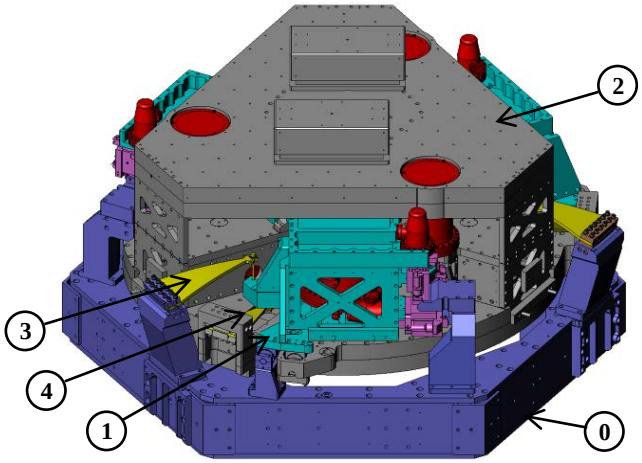

Figure 3. PROTOTYPE CAD PICTURE.

The system's architecture, geometrical and inertial properties are defined to minimize unwanted couplings, especially the tilt horizontal couplings. Stage 1 weighs a bit less than 1000 kg and Stage 2 weighs approximately twice as much. The rigid body modes are all between 1 Hz and 8 Hz. The two-stage configuration provides passive isolation in the 3 translation and 3 rotation directions, rolling off as the 4^{th} power of frequency above the natural rigid body resonances.

Six capacitive position sensors are used on each stage for the DC positioning and the low frequency control. Inertial instruments are used for the active seismic isolation. The first stage is instrumented with 3 low frequency three-axis seismometers, and 6 single-axis high frequency seismometers. Stage 2 is instrumented with 6 broadband seismometers. The active control scheme combines these position and inertial sensor signals to drive the electromagnetic actuators. Seismometers are shown in red in Figure 3. Position sensor and actuator blocks are shown in pink. The typical active seismic isolation bandwidth goes from 0.1 Hz to 30 Hz. Figure 4 shows the system prototype during the assembly process.

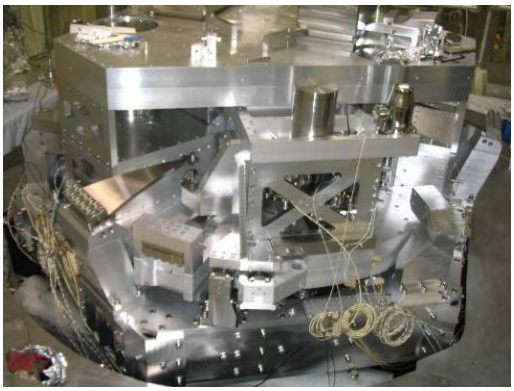

Figure 4. PROTOTYPE DURING ASSEMBLY PROCESS

2.3. Stage 1 Presentation

In this paper, we present the study and results obtained on the system's first stage. Figure 5 shows the aluminum structure (in grey) supported by the horizontal springs (1) and vertical flexures (2). The structure is threefold symmetric around the vertical axis. Each third of the structure includes:

- A horizontal actuator and position sensor block (3) and a vertical one (4).
- A horizontal (5) and vertical (6) single axis seismometer used at high frequency.
- A three-axis seismometer (7) used at low frequency.

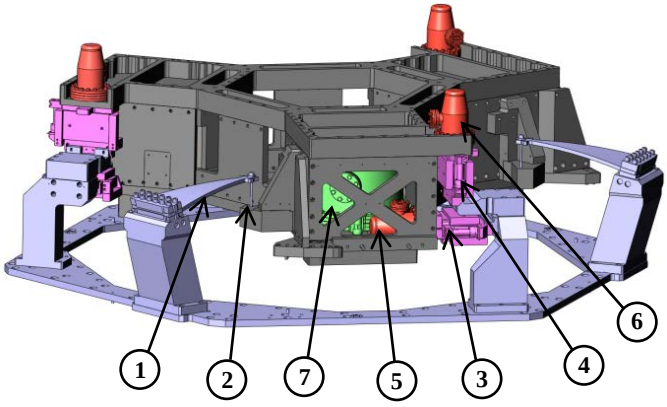

Figure 5. PROTOTYPE STAGE 1 ON SPRINGS AND FLEXURES. (STAGE 2 NOT SHOWN)

3. PROTOTYPING

3.1. Factors Limiting Performance

Figure 6 shows an example of a transfer function taken on the prototype's first stage after it was assembled and inserted in vacuum for the first time (Initial Prototype, 2008). It is compared with the theoretical response of an infinitely rigid stage (Model), which has the ideal behavior both for passive and active isolation performance.

In the experimental measurement (IP), the six actuators are combined to drive the stage in the X direction. The six single-axis seismometers are combined to sense the motion of the platform's geometrical center in the same direction. The rigid body mode resonances between 1 Hz and 8 Hz are actively damped. The first deformation mode is at 62 Hz, followed by three other large resonances below 100 Hz.

These modes limit the band of passive isolation. It is also one of the main limits to the platform's active isolation performance since the flexible modes have to either be controlled or filtered out of the feedback loop. The two solutions were investigated. They both make the compensators very complicated and highly sensitive to potential plants changes.

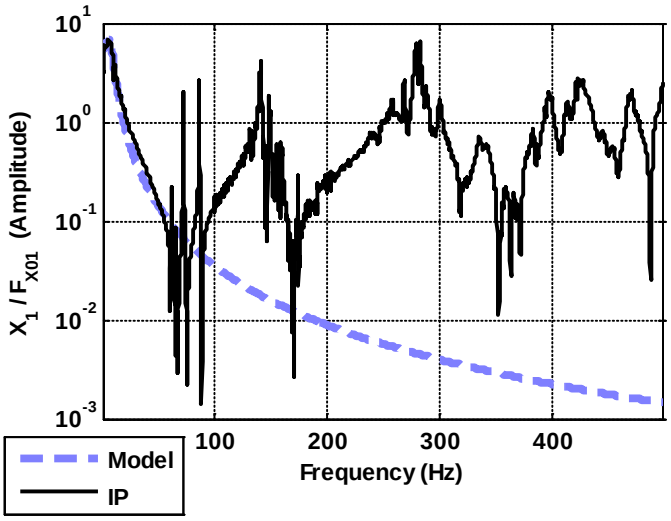

Figure 6. THEORETICAL IDEAL RESPONSE (MODEL) AND EXPERIMENTAL RESPONSE (INITIAL PROTOTYPE) IN THE X DIRECTION.

Figure 7 shows another example of transfer function, for the rotational response about the horizontal X axis (RX). The zoom on the 50 - 500 Hz band highlights the very high modal density. This transfer function shows more than 25 resonances below 300 Hz that must be accounted for in the controls design. Such a high modal density was observable in all degrees of freedom and was directly limiting the active control performance.

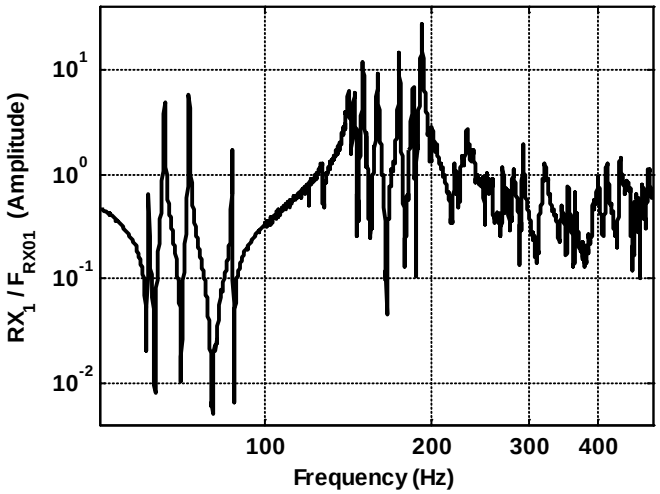

Figure 7. INITIAL PROTOTYPE RESPONSE, RX.

Another problem limiting the initial prototype performance was related to slow plant changes. The resonance frequencies have shifted by more than 1 Hz from one measurement to another, even though the platform was operating in an environmentally controlled ultra-high vacuum system. This behavior was observable in all six directions. Figure 8 shows an example of frequency shift between two measurements taken two months apart (Measurements A and B). The frequency shifts were due to the influence of small temperature changes on joints and boundary conditions. A high performance compensator based on the first measurement was unstable for the plant response in the second measurement.

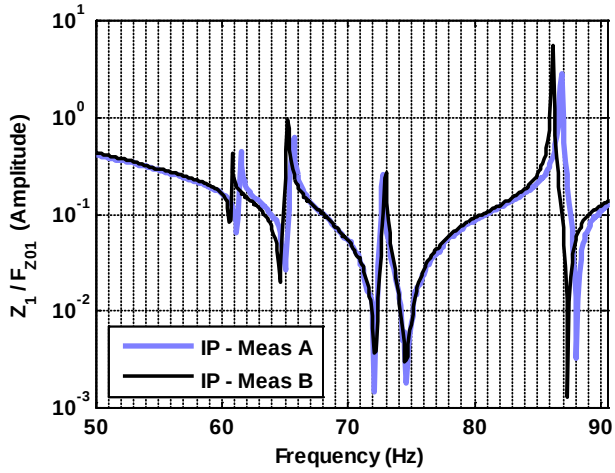

Figure 8. INITIAL PROTOTYPE, FREQUENCY SHIFTS.

Figure 9 shows an example of control implemented on the Initial Prototype, for the first stage rotation around the Y axis (RY). The relative position sensor and seismometer signals are combined to create a blended signal also called the "super-sensor" (RY in this example). The super-sensor signal is dominated by the position sensors from DC to about 0.1 Hz, by the low frequency seismometers from 0.1 Hz to 1 Hz, and by the high frequency seismometers above 1 Hz.

In Figure 9, the plant (P) is the transfer function from the torque (F_{RY}) to the super-sensor rotation (RY). The compensator (C) is the control filter between the controller input (RY) and output (F_{RY}). The open loop is the plant times the compensator (CP). The closed loop is the transfer function with the controller on: P/(1+CP).

In this example, all of the flexible modes are filtered out. Even with a conditionally stable compensator, and only 30 degrees of phase margin, the unity gain frequency was only at 20 Hz. This compensator contains a high number of notches and high frequency features, and is very sensitive to plant changes. Other options such as controlling the flexible modes were investigated, but were not suitable for robust long-term operations. The next section shows the investigation done on the prototype to improve its frequency response, the control performance and robustness.

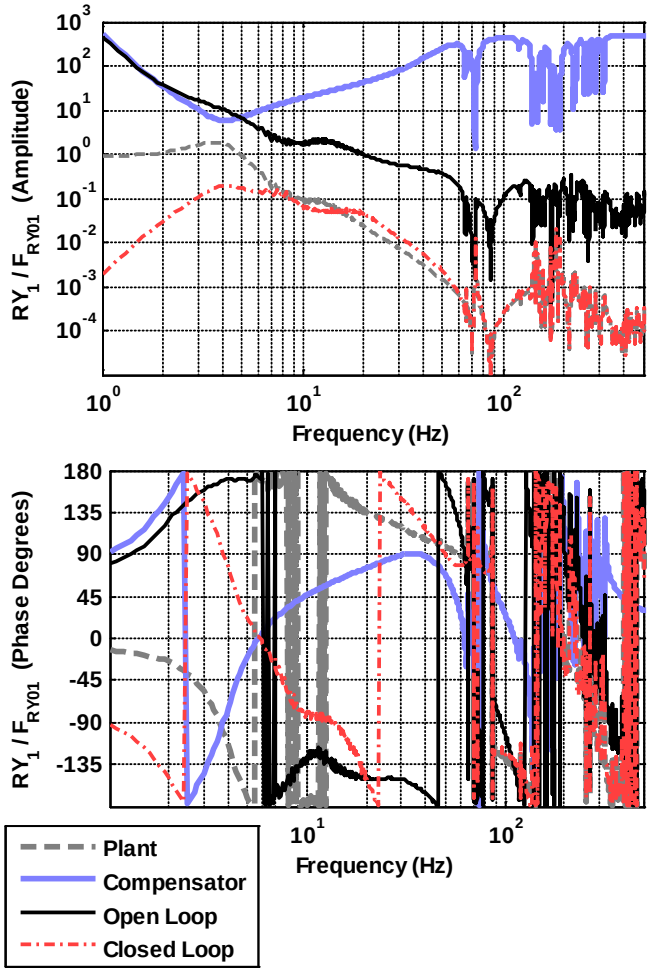

Figure 9. INITIAL PROTOTYPE, CONTROL IN RY.

3.2. Prototype Re-Engineering

Analytical and experimental analyses were done to understand and solve the three major issues identified: low frequency resonances, high modal density and plant changes.

Finite element analysis showed that the first global deformation modes should have been near 150 Hz, indicating that the lowest resonances identified experimentally were local deformation modes. We found them to be created by the counterbalance masses used to level the platform and by the cantilevered instruments. The counterbalance masses are necessary to compensate for uncertainties in the machining, spring materials properties, and discrepancies between theoretical analysis and actual system compliance. The spring position and angles were adjusted to improve the platform leveling and therefore reduce the amount of mass needed for static balancing (reducing it from 390 lbs to 95 lbs). The instrument attachment has been re-engineered to stiffen and minimize local resonances.

Figure 10 shows the improvement obtained in the prototype transfer function after these re-engineering operations. The X direction is used as an example. The prototype re-engineering raised the lowest resonances to 130 Hz and solved the plant frequency shifts. Similar improvements were obtained in all six directions.

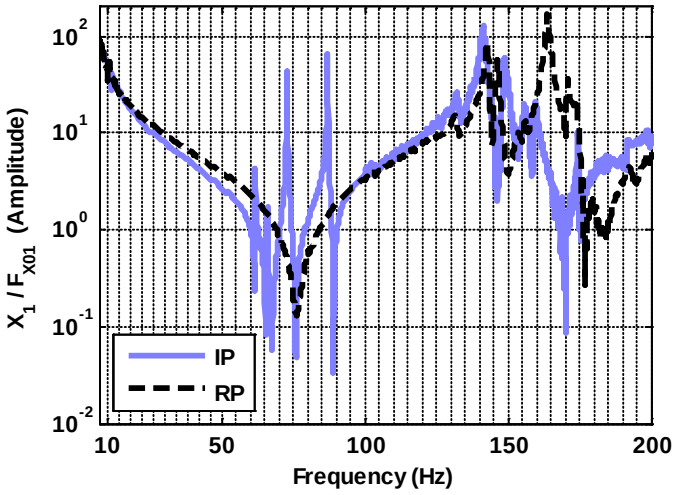

Figure 10. INITIAL PROTOTYPE (IP) AND RE-ENGINEERED PROTOTYPE (RP) RESPONSE.

The control loops have been re-designed to evaluate the impact of the re-engineering on the controllers performance and complexity. Figure 11 shows the control in the RY direction after prototype re-engineering, for comparison with the controller presented in Figure 9 (Initial Prototype). The controller design used a quasi plant inversion approach to filter out the high frequency resonances while minimizing the phase loss, as shown in Figure 11. With such an "aggressive" controller, we were able to raise the unity gain frequency near 30Hz, but with only 30 degrees of phase margin.

Comparison with the results obtained with the Initial Prototype (Figure 9) show that the re-engineering made the compensator simpler and helped improve the control bandwidth. The complexity of the controllers, the sensitivity to plant changes, and the lack of robustness remained however not suitable for the commissioning of 15 units necessary for the Advanced LIGO observatory. The next section shows the analysis and re-design undertaken to design the system's final version with an improved the dynamic response.

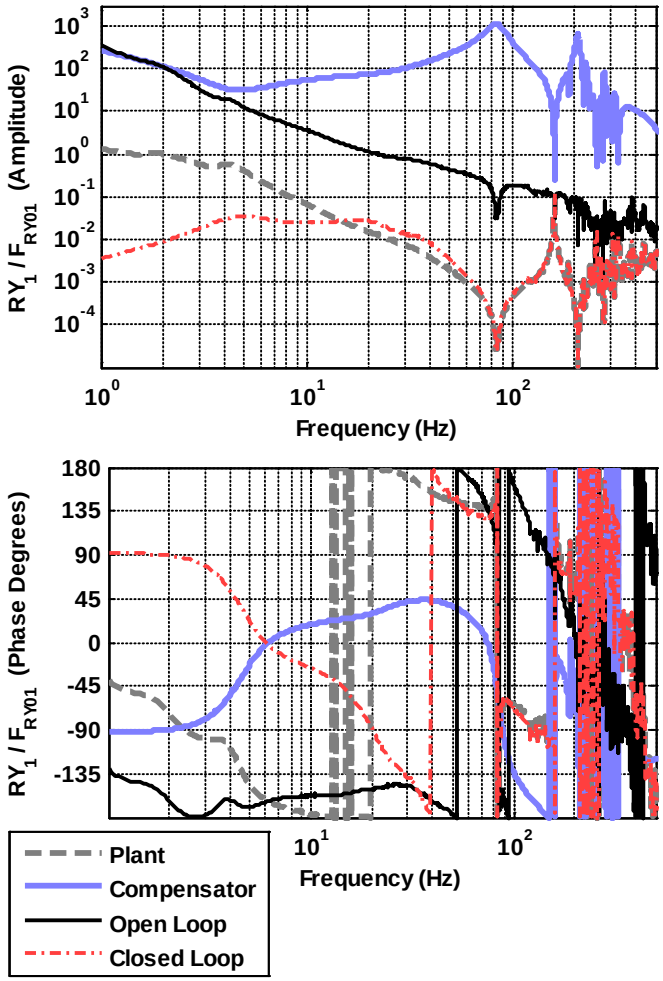

Figure 11. RE-ENGINEERED PROTOTYPE, CONTROL IN RY.

4. FINAL DESIGN

4.1. Sensors Re-Location

It is usually a good practice to collocate actuator and sensor pairs, as shown in Figure 12 where horizontal actuators and seismometers are collocated (1), such as the vertical ones (2). In principle, this technique simplifies the feedback control loop since the transfer functions alternate poles and zeros, and consequently minimizes the phase loss.

The prototype commissioning has however shown that controlling the high frequency modes (100 Hz and above) requires near perfect plant inversion. Implementing such control will not be suitable for Advanced LIGO since the 15 units that will be used during operations must rely on very robust controllers. We consequently investigated the benefits of relaxing the collocation requirements.

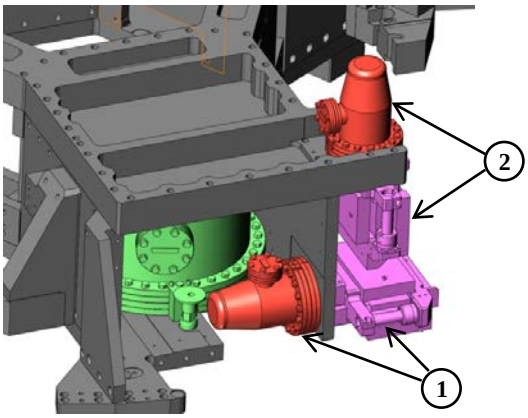

Figure 12. COLLOCATED SENSOR/ACTUATOR PAIRS.

The prototype's Finite Element Analysis (FEA) showed that the collocated vertical sensor and actuator motion were locally amplified by the cantilevered mass, even on the lowest mode as shown in Figure 13. Relaxing the colocation criteria allows the sensors to be placed in stiffer locations and reduces the cantilevered mass.

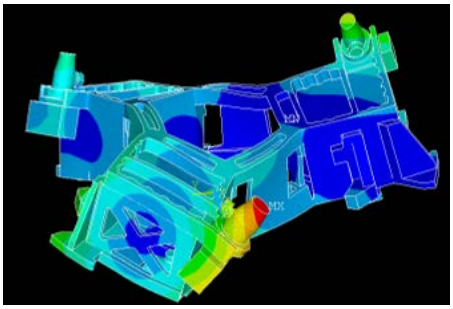

Figure 13. PROTOTYPE FEA, FIRST MODE.

For the horizontal instrument, the colocation required a large cutout in the base plate, reducing the structural stiffness. Relaxing the colocation requirements allowed us to reposition the sensors near the center of rotation of the arm-twist modes. Figure 14 shows how the instruments have been repositioned. The vertical sensor is no longer mounted on the cantilevered area (1). The horizontal instrument has been raised (2) thus allowing a much stiffer connection between the baseplate and the vertical wall (3).

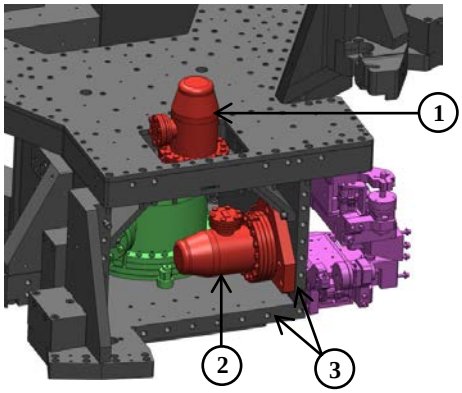

Figure 14. SENSOR RELOCATION.

The FEA results in Figure 15 show that the instruments have been repositioned in areas of lower motion (blue areas of low displacement).

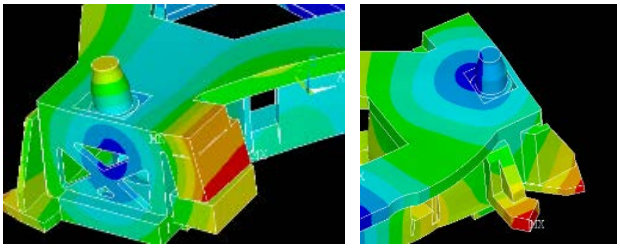

Figure 15. FEA RESULTS AFTER SENSORS RELOCATION

4.2. Stiffening

The prototype's lowest resonance was estimated at 151 Hz with the FEA model, and measured at 131 Hz on the prototype after the re-engineering presented in the previous section. The FEA results in Figure 13 show that the lowest resonance was a torsional arm-twist mode.

Figure 16 shows the re-design of the close out plate. The black contour (1) shows the material added to reinforce the global torsion modes (around the blue arrow) and the global bending modes (along the blue arrow). Successive design/FEA iterations showed that extending the plate beyond the red arrow would create local bending modes. The configuration shown below gave the optimal compromise. The webbing (2) was designed to increase the stiffness over mass ratio.

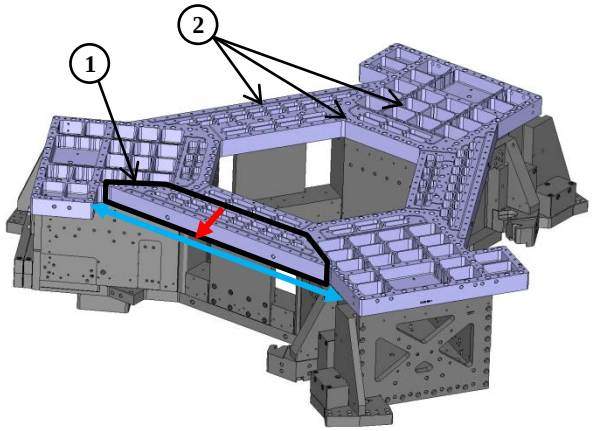

Figure 16. CLOSE OUT PLATE REDESIGN.

Figure 17 highlights the other major design improvements. A cover plate has been added to improve the structure resistance to bending (3). The actuator mounting has been redesigned to increase the local stiffness (4). A central block (5) has been designed to improve the resistance to torsion that was very low in this area (black arrows). Additional counterbalance mass locations have been added (6), to provide stiff mounting if additional mass is necessary for leveling the stage. Corner brackets were added to reduce local deformation between the walls and the top plate (7). The initial design included a 94 lbs

stainless steel ballast (8) to align the center of gravity with the actuator plane. This requirement could be relaxed, which allowed use of much lighter ballast mass (31 lbs aluminum). The base plate was stiffened (9) after seismometer relocation as described in the previous section.

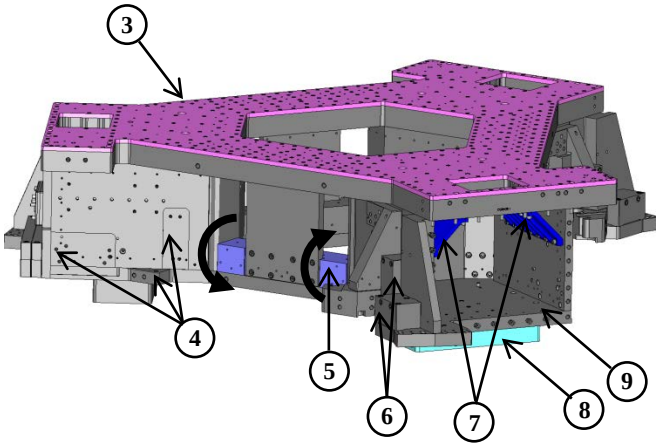

Figure 17. STRUCTURAL IMPROVEMENT HIGHLIGHTS.

Figure 18 shows the first and second flexible bending modes of the Final Design (FD). The design changes helped to raise the first mode (arm-twist) from 151 Hz (Figure 13) to 255 Hz (Figure 18.a). They helped to raise the second mode (arm-in-plane bending) from 155 Hz to 302 Hz (Figure 18.b). The third and fourth modes predicted by the FEA on the original prototype were horizontal actuator modes at 166 Hz and 192 Hz. The third and fourth modes predicted on the new design are global deformation modes at 326 Hz and 364 Hz.

(a)

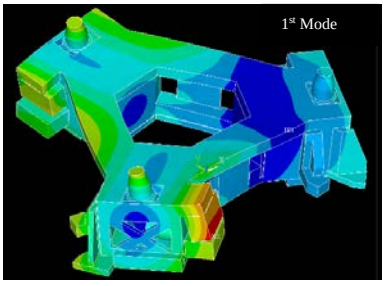

(b)

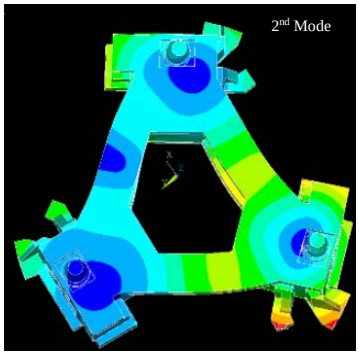

Figure 18. FINAL DESIGN FEA, FIRST AND SECOND FLEXIBLE MODES.

Figure 19 shows the first stage new design including all the changes described in this section. The next section shows the corresponding experimental modal analysis results.

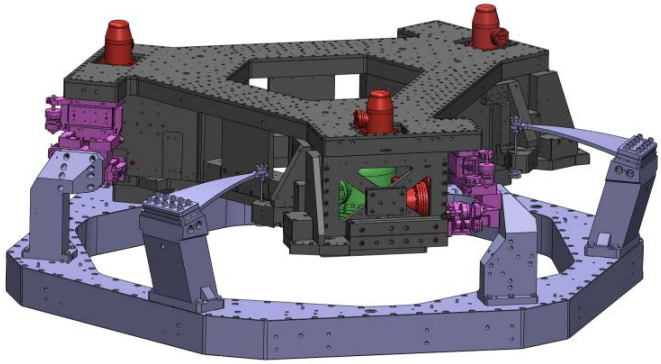

Figure 19. CAD OF THE FINAL DESIGN (SECOND STAGE NOT SHOWN).

5. FINAL DESIGN EXPERIMENT AND CONTROL

5.1. Experimental modal analysis and passive damping

Figure 20 shows the new first stage, and the experimental setup used to identify the structure resonances. The structure is suspended with a three-point lift. Accelerometers are mounted on the sidewalls. An impact hammer with force sensor is used to excite the structure and a spectrum analyzer is used to process the transfer functions.

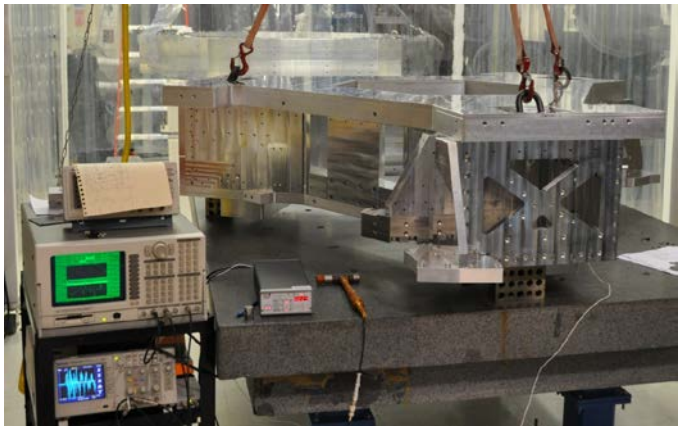

Figure 20. MODAL ANALYSIS SET UP

Initially, the structure was tested without instruments to characterize the structural assembly. The first resonance was measured at 278 Hz, demonstrating the very high structural stiffness of the final design.

Figure 21 shows the structure instrumented with Trilliums (1) and L4Cs (2). In this configuration, the lowest resonance was measured to be at 262 Hz. This compares well with the lowest FEA predicted mode at 255 Hz, though the FEA included actuators that were not present in the experimental test (they had not arrived from the manufacturer when the test took place).

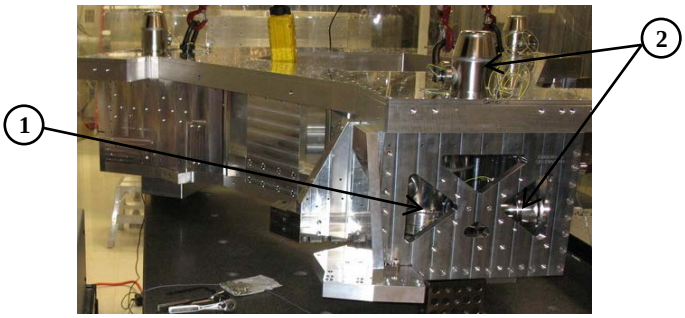

Figure 21. INSTRUMENTED STAGE

Tuned mass dampers were installed in order to lower the Qs of the first flexible modes. Figure 22 shows 10 lbs masses mounted on Viton pads in each of the three arms. The Viton acts as a spring-damper. The mass spring damper systems are tuned near the structural resonances. This reduced the quality factor of the first resonance by a factor of 20 (Figure 23). Similar vibration absorbers were included in the final design. Figure 22 (right) shows the final design of the vibration absorbers installed on the front door.

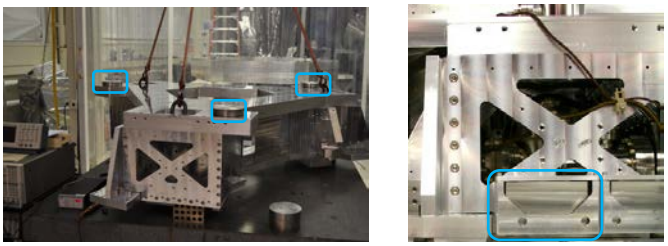

Figure 22. PRELIMINARY DAMPING TESTS (LEFT) AND VIBRATION ABSORBERS FINAL DESIGN (RIGHT)

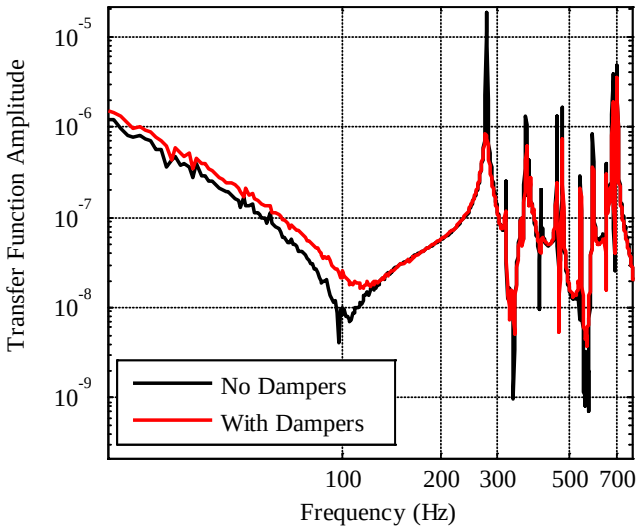

Figure 23. MODAL ANALYSIS RESULTS.

5.2. Transfer function improvements

Figure 24 shows the two-stage platform final design, fully assembled at the LIGO Hanford observatory.

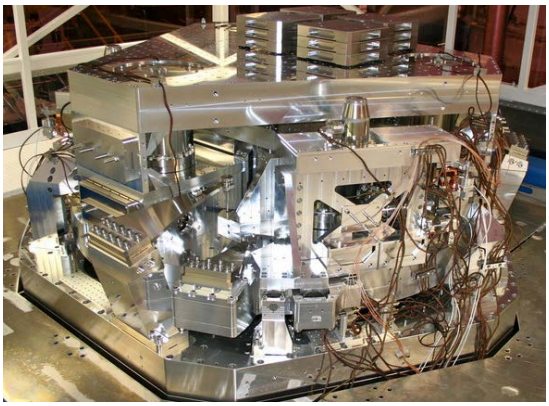

Figure 24. TWO-STAGE PLATFORM FINAL DESIGN.

Figure 25 compares the transfer functions in the X direction, obtained with the Re-engineered Prototype, and with the Final Design. The lowest significant resonance is at 214 Hz. This value is a bit lower than in the modal test results shown in the previous section because of the change of boundary conditions: stage 1 simply suspended in the modal analysis (Figure 23), versus stage 1 connected to Stage 0 and Stage 2 in full assembly's transfer functions (Figure 25). The comparison of the red curve and the black curve in Figure 25 shows the significant improvement obtained with the Final Design.

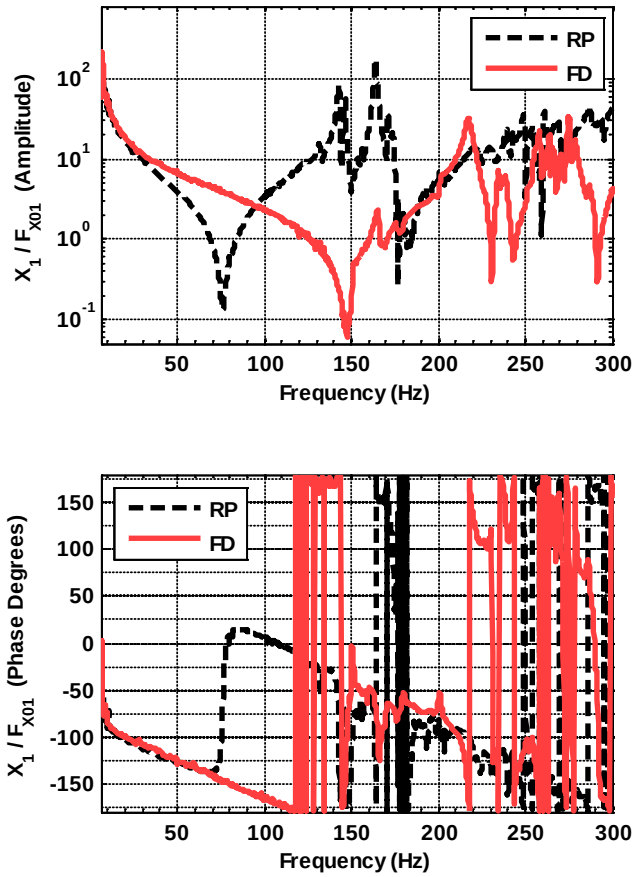

Figure 25. COMPARISON OF RE-ENGINEERED PROTOTYPE AND FINAL DESIGN.

5.3. Control Results

Figure 26 shows an example of control for the Final Design structure. It shows the control in the RY direction for comparison with the controller presented in Figure 9 (Initial Protoype) and Figure 11 (Re-engineered Protoype). The unity gain frequency is 30 Hz with 30 degrees of phase margin The open loop shows it is a conditionally stable compensator. The plant shows that the stage provides a slightly lower passive isolation than the prototype (lower inertia) but a much simpler frequency response. Therefore, high performance and robustness can be obtained with a very simple compensator.

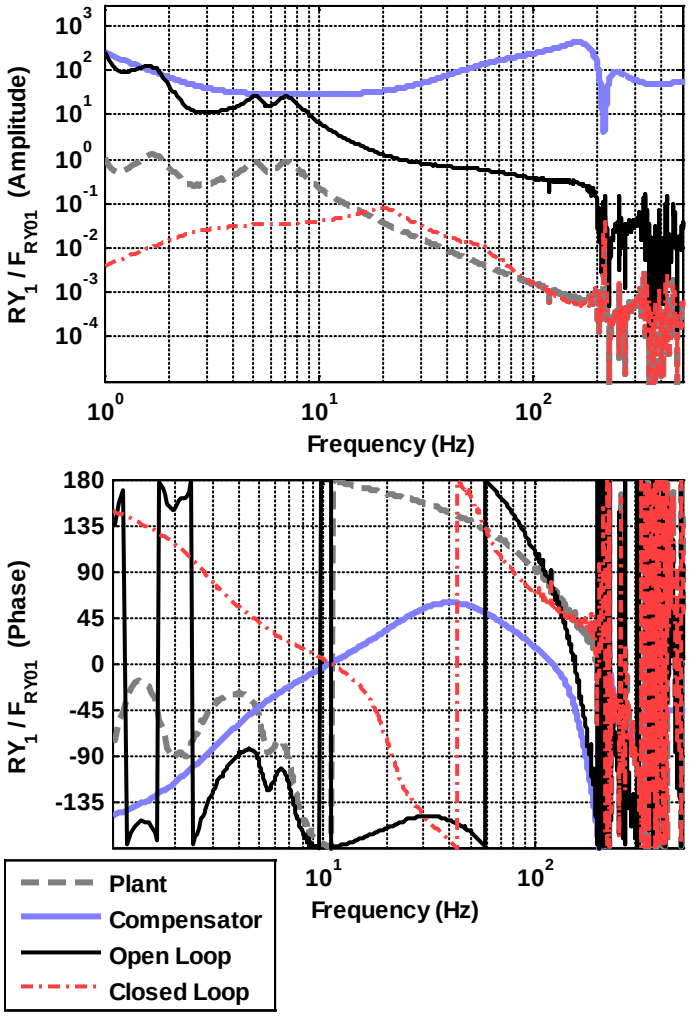

Figure 26. FINAL DESIGN, CONTROL IN RY.

The plots in Figure 27 compare the compensators used during the three phases of this project. Semi-log plots are used to zoom on the high frequency features. Figure 27.a illustrates the high number of notches that were needed to filter out the Initial Prototype's resonances (2008). The compensator was made of 104 poles and zeros.

Figure 27.b shows a compensator used during the prototype re-engineering phase (2009-2010). A quasi plant inversion (64 poles and zeros) was used to reach a 30 Hz unity gain frequency, at the cost of development time and robustness loss.

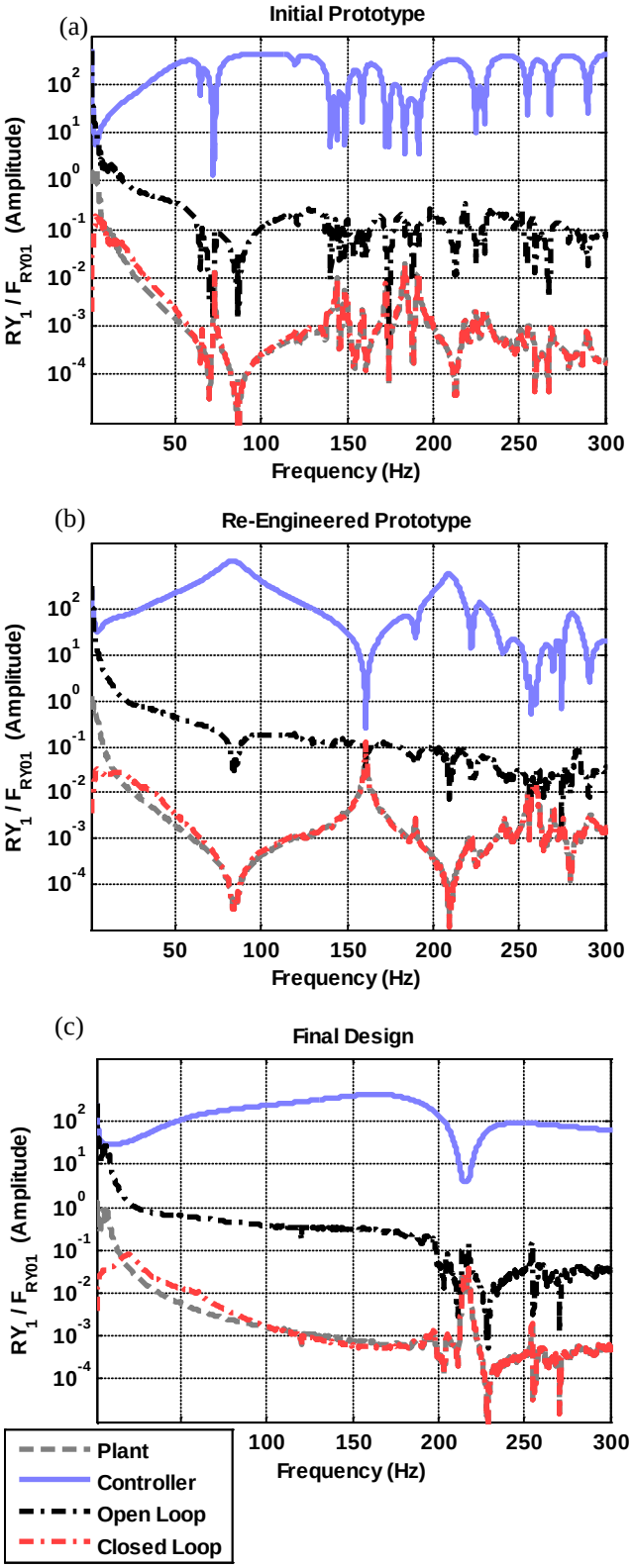

Figure 27. CONTROLLERS COMPARISON.

Figure 27.c shows a control loop used on the Final Design (2011). The compensator is significantly simpler than any used on the prototype. It is made of 22 poles and zeros (5 pairs of complex conjugate zeros and 6 pairs of complex conjugate poles). The order of the controller has therefore been significantly reduced. The compensator and open loop curves show that a 30 Hz unity gain frequency can be obtained with a single notch on the main resonance at 214 Hz. This Final Design will help not only to improve the active control performance but also to greatly speed up the commissioning of the 15 units that will be used for Advanced LIGO.

CONCLUSION

The goal of this program was to study and improve the two-stage vibration isolator concept designed for the Advanced LIGO observatory. A prototype was built and analyzed (Initial Prototype, 2008). The three main factors limiting the active control performance were identified. They were the low frequency deformation modes, the high modal density and plant changes. Improvements done on the prototype have been presented (Re-Engineered Prototype, 2009). The work done on counterbalance mass mounting and weight reduction, and sensor attachment improved the prototype dynamics. A quasi-plant inversion approach was used to reach a 30 Hz unity gain frequency in all 12 degrees of freedom. The complexity of the controllers, the sensitivity to plant changes, and the lack of robustness were however not meeting requirements.

A major re-design was then undertaken to make the structure suitable for Advanced LIGO (Final Design, 2010-2011). The goal was not only to improve the active control performance, but also to increase robustness necessary for operation. The first stage re-design study has been detailed. Experimental results obtained with this Final Design showed the structural resonance improvements. The transfer functions taken on the first unit assembled showed a lowest resonance at 214 Hz, compare to 61 Hz on the Initial Prototype, and 131 Hz on the Re-engineered Prototype. The comparison of controllers used during the three phases of this study illustrates the performance improvements obtained, and the simplification of the compensators, which will speed up the commissioning of Advanced LIGO, and increase the system robustness.

ACKNOWLEDGMENTS

LIGO was constructed by the California Institute of Technology and the Massachusetts Institute of Technology with funding from the National Science Foundation and operates under cooperative agreement PHY-0107417. This document has been assigned LIGO Laboratory document number LIGO-P1200011

We acknowledge the JILA group who provided the original concept and ASI for the prototype design.

This work would not have been possible without the outstanding support of the LIGO laboratory management, procurement, quality assurance, FMP, assembly, installation, CDS and testing teams.

REFERENCES

[1] Harry, G. M., et al., 2010, “Advanced LIGO: The Next Generation of Gravitational Wave Detectors”, Classical and Quantum Gravity, **27,** 084006.

[2] Grote, H., et al., 2010, “The GEO600 Status,” Class. Quantum Grav, **27**, 084003.

[3] Acernese, F., et al., 2008, “Status of Virgo,” Class. Quantum Grav., **25**, 114045.

[4] Arai K., et al., 2009, “Status of Japanese Gravitational Wave Detectors,” Class. Quantum Grav, **26**, 204020.

[5] Abbott R., et al., “Seismic Isolation Enhancements for Initial and Advanced LIGO,” Class. Quantum Grav., **21**, pp. 915-921.

[6] Robertson, N. A., et al., 2004, “Seismic Isolation and Suspension Systems for Advanced LIGO,” Gravitational Wave and Particle Astrophysics Detectors, Proceedings of SPIE, pp. 81-91.

[7] Robertson, N. A. et al., 2002, “Quadruple Suspension Design for Advanced LIGO,” Class. Quantum Grav., **19**, pp. 4043-4058.

[8] Matichard, F., et al., 2010, “Prototyping, Testing, and Performance of the Two-Stage Seismic Isolation System for Advanced LIGO Gravitational Wave Detectors,” Proceedings of ASPE conference on Control of Precision Systems, pp. 75-80.

